Nonsensory target-dependent organization of piriform cortex

Chien-Fu F. Chen[a], Dong-Jing Zou[a], Clara G. Altomare[a], Lu Xu[a], Charles A. Greer[b], and Stuart J. Firestein[a,1]

[a]Department of Biological Sciences, Columbia University, New York, NY 10027; and [b]Neuroscience Program, Yale University School of Medicine, New Haven, CT 06520

Edited by Joseph E. LeDoux, New York University, New York, NY, and approved October 22, 2014 (received for review June 18, 2014)

The piriform cortex (PCX) is the largest component of the olfactory cortex and is hypothesized to be the locus of odor object formation. The distributed odorant representation found in PCX contrasts sharply with the topographical representation seen in other primary sensory cortices, making it difficult to test this view. Recent work in PCX has focused on functional characteristics of these distributed afferent and association fiber systems. However, information regarding the efferent projections of PCX and how those may be involved in odor representation and object recognition has been largely ignored. To investigate this aspect of PCX, we have used the efferent pathway from mouse PCX to the orbitofrontal cortex (OFC). Using double fluorescent retrograde tracing, we identified the output neurons (OPNs) of the PCX that project to two subdivisions of the OFC, the agranular insula and the lateral orbitofrontal cortex (AI-OPNs and LO-OPNs, respectively). We found that both AI-OPNs and LO-OPNs showed a distinct spatial topography within the PCX and fewer than 10% projected to both the AI and the LO as judged by double-labeling. These data revealed that the efferent component of the PCX may be topographically organized. Further, these data suggest a model for functional organization of the PCX in which the OPNs are grouped into parallel output circuits that provide olfactory information to different higher centers. The distributed afferent input from the olfactory bulb and the local PCX association circuits would then ensure a complete olfactory representation, pattern recognition capability, and neuroplasticity in each efferent circuit.

olfaction | piriform cortex | olfactory perception

The olfactory system creates perceptual odor objects from often complex mixtures of diverse airborne chemicals (1, 2). This formidable job is mainly accomplished by a surprisingly "shallow" three-level pathway, comprising the olfactory epithelium, olfactory bulb, and olfactory cortex (3). The olfactory epithelium accommodates millions of olfactory sensory neurons (OSNs), each of which can be defined by the particular receptor protein selected for expression from the ∼1,000 odor receptor genes in the typical mammalian genome (4, 5). Axons from all OSNs expressing the same odor receptor coalesce into a few glomeruli on the surface of the olfactory bulb (6–8). Each glomerulus is therefore dedicated to a particular receptor. The position of each glomerulus appears to vary only slightly from animal to animal, giving rise to speculation that the glomeruli form a spatial map of odor sensitivities.

Within the glomeruli, the incoming OSN axons form synapses with the apical dendrites of second-order neurons and the mitral and tufted cells, providing what would seem to be an anatomical basis for topographical odorant representation (9–11). Each of about a dozen mitral or tufted cells innervating only a single glomerulus send their axons to targets in a number of ventral forebrain areas, collectively termed the olfactory cortex (12).

However, this seemingly orderly topography of odorant representation is not maintained in the olfactory cortex. Especially in the largest olfactory area—the piriform cortex (PCX)—odorants are represented by sparse, distributed, and spatially overlapping neural ensembles across the cortex (13–18). This nontopographical representation stems largely from the architecture of the PCX, including distributed afferent inputs (19–21), and a similarly distributed intracortical association fiber system, which links single cortical neurons (pyramidal and semilunar cells) with neighboring and distant neurons (22–25). Furthermore, each cortical neuron receives an apparently random collection of glomerular inputs (26, 27). Therefore, a spatial location of the cortex is not predictive of odorant tuning as neighboring neurons may exhibit distinct receptive ranges (14, 18, 27).

Compared with existing data on the afferent and association connections, data on the efferent aspects of PCX are limited. Although previous studies have identified a number of higher centers that are targeted by the PCX output neurons (OPNs), including the orbitofrontal cortex (OFC), hippocampus, hypothalamus, and thalamic nuclei (28–31), information regarding organization and spatial distribution of these neurons (pyramidal and semilunar cells) is lacking. Questions such as how the OPNs projecting to different targets are distributed within PCX and whether that may imply any intrinsic or functional organization of the PCX remain unanswered. Given the complexity of the distributed afferent and association fiber system, data from the efferent system may help to discern organizing principles in the PCX and lend some understanding as to how it processes incoming sensory information.

To reach this goal, we focused on the projection from the PCX to the OFC, an important center for odor-guided behaviors (19, 30, 32). We injected different cholera toxin B (CTB) subunit fluorescent conjugates into two subdivisions of the OFC, the agranular insular (AI) and the lateral OFC (LO), in mice and examined the PCX for retrograde labeling (33). We found that the OPNs projecting to the AI and the LO are differentially

Significance

The mammalian olfactory system is capable of detecting and discriminating a vast and diverse array of small organic molecules or odorants. Complex blends of these chemicals are finally perceived as a unified odor object—for example, a rose contains dozens of active compounds. The piriform cortex (PCX) is the largest component of the olfactory cortex and has been hypothesized to be the locus of odor object formation. However, the PCX shows a distributed odorant representation that contrasts sharply with the topographical representation typically seen in the other primary sensory cortices. In this article, we explore an alternative organizational principle for the PCX based on where neurons are sending their output, rather than where these neurons are receiving their input.

Author contributions: C.-F.F.C. and S.J.F. designed research; C.-F.F.C., D.-J.Z., and L.X. performed research; C.-F.F.C., D.-J.Z., C.G.A., L.X., and C.A.G. analyzed data; and C.-F.F.C., D.-J.Z., C.A.G., and S.J.F. wrote the paper.

The authors declare no conflict of interest.

This article is a PNAS Direct Submission.

[1]To whom correspondence should be addressed. Email: sjf24@columbia.edu.

This article contains supporting information online at www.pnas.org/lookup/suppl/doi:10.1073/pnas.1411266111/-/DCSupplemental.

NEUROSCIENCE

distributed. Interestingly, both OPNs to the AI and LO exhibited topographically specific distributions in the PCX. In addition, they showed distinct distribution patterns along the anterior–posterior axis of the PCX. These two OPN populations had limited overlap within the anterior PCX (aPCX), as double-labeled neurons were extremely rare. These data suggest that the functional organization of PCX may be better understood through its output circuits, shedding new light on the role of olfactory cortex in central odor processing.

Results

CTB Retrograde Tracing Confirmed Neural Connectivity of the OFC. To examine the quality of the CTB injections, we checked locations of the injection sites, along with the CTB labeling in areas that project directly to the OFC, including the mediodorsal (MD) and the submedius (Sub) thalamic nuclei, the lateral and the basolateral amygdaloid nuclei, the endopiriform nucleus, and the PCX (30, 34, 35). We first confirmed that the injection sites of all five animals were confined in the AI and/or the LO (Fig. 1 *A* and *D*). In each animal, the CTB-positive cells were identified in the MD and the Sub thalamic nuclei, although some AI projecting neurons were also found in the ventromedial thalamic nucleus (Fig. 1*B*). CTB-positive cells in the ventral forebrain areas included the lateral and the basolateral amygdaloid nuclei (Fig. 1*C*), the endopiriform nucleus (Fig. 2 *A*, *B*, *E*, and *F*), and the PCX (Fig. 2). Together, these data confirmed the previous findings on the neural connectivity of the OFC and suggested the injections were in the correct locations.

OPNs of the PCX Showed Topographical Distributions. We examined the CTB-positive cells through a series of coronal sections within three PCX subdivisions, from anterior to posterior: rostral aPCX, middle/caudal aPCX, and posterior PCX (pPCX). LO-OPNs (the OPNs projecting to the LO) were labeled by either CTB-647 or CTB-555 (*Materials and Methods*), and the distribution patterns appeared to be independent of the two tracer conjugates (Fig. 2*D*). The data showed that LO-OPNs were not evenly distributed but concentrated in specific compartments in all three subdivisions of the PCX (Fig. 2 *A–C* and Table 1). The rostral aPCX is characterized by a dense layer II, which includes a dorsal (regions 3 and 4) and a ventral band (regions 1 and 2) (*Materials and Methods* and Fig. 2*A*). Following the LO injections, 62 ± 4% (mean ± SEM) of the labeled LO-OPNs were found in region 1 and 27 ± 4% in region 4 of the rostral aPCX. Only 8 ± 1% and 3 ± 0% of the cells were in regions 2 and 3, respectively (Fig. 2*D*, *Left*). In the middle/caudal aPCX, where the layer II dorsal band is not present, LO-OPNs were distributed similarly; 78 ± 3% of the cells were in region 1 and 22 ± 3% in region 2 (Fig. 2*D*, *Center*). The pPCX of the mouse begins when the myelinated M/T-cell axons (the lateral olfactory tract, or LOT) are no longer well delineated. Very few LO-OPNs were identified in the pPCX (Table 1), suggesting a very weak projection from the pPCX to the LO. In this population, 79 ± 12% of the cells were in region 1 and 21 ± 12% in region 2 (Fig. 2*D*, *Right*). Together, the nonrandom or compartmental distribution derived from these data indicates that a topographically organized efferent system may exist in the PCX. AI-OPNs (the OPNs projecting to the AI) also showed a topographical distribution (Fig. 2 *E–H* and Table 2). Similar to LO-OPNs, AI-OPNs in the rostral aPCX were located largely in regions 1 (39 ± 4%) and 4 (44 ± 4%), with only 13 ± 2% and 4 ± 1% of the cells in regions 2 and 3, respectively (Fig. 2 *E* and *H*, *Left*). Distribution patterns of AI-OPNs were similar in the middle/caudal aPCX and pPCX, where the cells were mainly located in region 1 (69 ± 2% and 82 ± 3%, respectively) (Fig. 2*H*, *Center* and *Right*). Collectively, these data demonstrate that although the afferent projections from the olfactory bulb to PCX appear to lack a topographical foundation (20), the efferent output from PCX OPNs has a segregated connectivity correlated with subdivisions of the OFC.

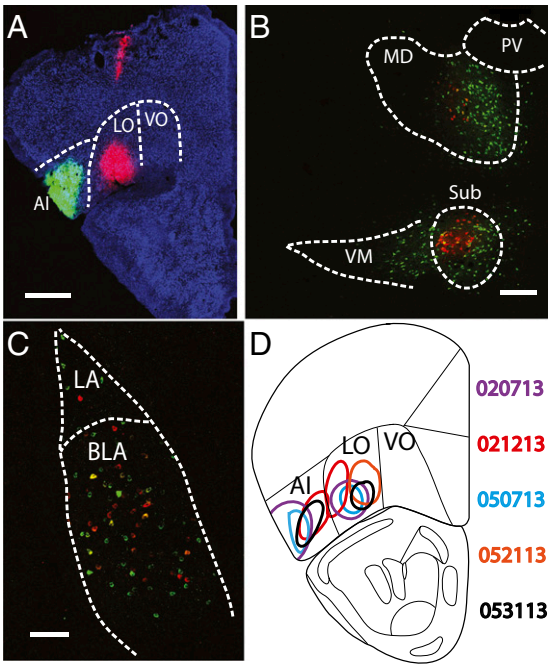

Fig. 1. CTB retrograde tracing in the mice. (*A*) The injection sites of mouse 020713. AI, CTB-555 (green); LO, CTB-647 (pink); background, NeuroTrace Blue. Both AI (green) and LO (pink) projecting neurons are located in the thalamic nuclei (*B*) and the amygdaloid nuclei (*C*). (*D*) Injection sites of all five animals drawn on a coronal section 2.68 mm anterior to the bregma. Outlines were reproduced from ref. 46. AI, agranular insular; BLA, basolateral amygdaloid nucleus; LA, lateral amygdaloid nucleus; LO, lateral OFC; MD, mediodorsal thalamic nucleus; PV, paraventricular thalamic nucleus; Sub, submedius thalamic nucleus; VM, ventromedial thalamic nucleus; VO, ventral OFC. (Scale bar, 200 μm.)

Target-Dependent OPN Patterns on the Anterior–Posterior Axis of the PCX. We next studied the distributions of OPNs targeting the OFC along the anterior–posterior axis of the PCX. Data from LO-OPNs and AI-OPNs in each animal were smoothed and normalized to assess the anterior–posterior distributions (*Materials and Methods*). LO-OPNs were predominately located in the aPCX (pink line in Fig. 3*A*). The cell numbers abruptly decreased at the border of the middle/caudal aPCX. In contrast with LO-OPNs, the distribution of AI-OPNs fluctuated across the aPCX and gradually decreased in the pPCX (green line in Fig. 3*B*).

To assess this further, the CTB-positive cells of the mouse 020713 were plotted on the flattened PCX (Fig. 3*C*). In this presentation, two obvious LO-OPN clusters were located in the medial aspect of the dorsal layer II band (region 4) and the ventral portion of the ventral band (region 1) of the rostral aPCX. AI-OPNs interdigitated with LO-OPNs in the rostral aPCX and the initial third of the middle/caudal aPCX. Posteriorly, the PCX was predominately occupied by AI-OPNs, as is particularly evident in the ventral PCX. Consistent patterns of both AI-OPNs and LO-OPNs were observed in other animals (Fig. S1). Together, these data showed distinct OPN patterns that were dependent on the cells' targets.

LO- and AI-OPNs Belong to Different Output Circuits. We then asked whether OPNs had overlapping projections to the AI and the LO such that single cells may project to both areas. To answer this question, we examined the percentage of the cells that were colabeled with CTB-555 and CTB-647 following injections into the AI and the LO. In addition, we determined quantitatively the

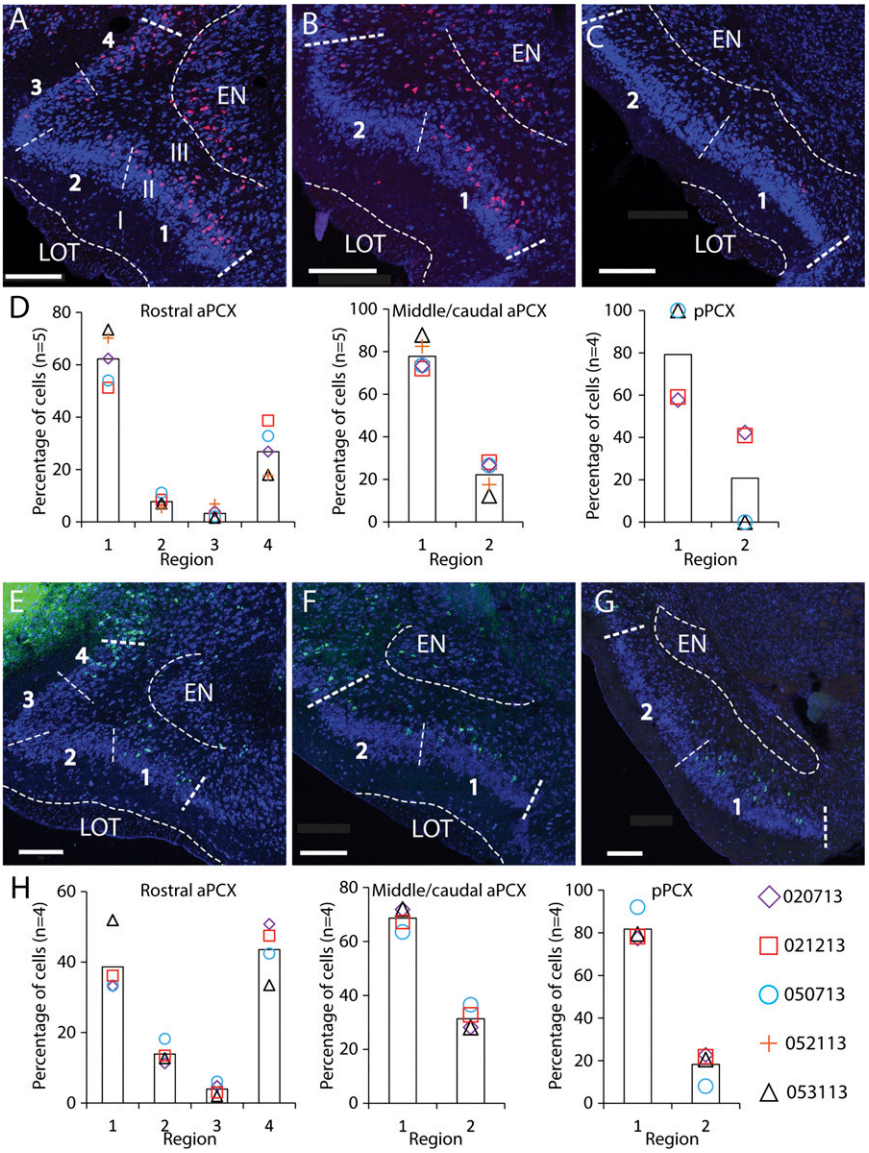

Fig. 2. Distributions of LO- and AI-OPNs in coronal sections of the PCX. (*A*) An example of LO-OPNs (pink, CTB-647) in the rostral aPCX. The ventral band of the aPCX is divided into regions 1 and 2. The dorsal band of the aPCX comprises regions 3 and 4 (*Materials and Methods*). (*B* and *C*) The cell distributions in the middle/caudal aPCX where *B* is anterior to *C*. (*D*) Regional distributions of LO-OPNs in the rostral aPCX (*Left*), the middle/caudal aPCX (*Center*), and the pPCX (*Right*). Data of individual animals were shown in the lines of different colors. (*E–G*) Examples of AI-OPN (green, CTB-555) distribution in the rostral aPCX, the middle/caudal aPCX, and the pPCX, respectively. (*H*) Regional distributions of AI-OPNs in the rostral aPCX (*Left*), the middle/caudal aPCX (*Center*), and the pPCX (*Right*). The thin white dashed lines mark the regional boundaries, and the thick white dashed lines mark the boundaries of the PCX. *I*, *II*, and *III*, lamination of the PCX. EN, endopiriform nucleus; LOT, lateral olfactory track. (Scale bar, 200 μm.)

spatial or topographical overlap of LO-OPNs and AI-OPNs in the PCX. Cells of the two populations that located in the same 100 μm × 100 μm squares were defined as within an overlapping domain (Fig. 3*D*). We found that only 12 ± 2% of labeled neurons in the rostral aPCX were double-labeled with both CTB conjugates, indicating that they sent efferent axon collateral to both OFC subdivisions (Fig. 3*E*). The average colabeling percentages dropped to 7 ± 3% and 1 ± 1% in the middle/caudal aPCX and the pPCX, respectively. Overall, only 8 ± 2% of the CTB-positive cells were double-labeled following the LO and the AI injections. This low percentage of double-labeled cells was unlikely due to the low labeling efficiency of either tracer. When a mixture of CTB555 and CTB647 (in equal amounts) was simultaneously injected in the OFC, CTB-positive cells in the PCX were 99% double-labeled by both tracers (Fig. S2).

In contrast to the paucity of double-labeled cells, 59 ± 8% of the labeled LO-OPNs and AI-OPNs in the rostral aPCX were found within the overlapping domains defined by the 100-μm grids (Fig. 3*E*). These two OPN populations also intermingled (48 ± 7%) in the middle/caudal aPCX. In the pPCX, the frequency of overlapping within a domain dropped to 7 ± 4%, perhaps in part because of the infrequent distribution of LO-OPNs in the pPCX (Fig. 3*A*). Overall, the frequency of overlap within domains was 48 ± 7%, indicating that the two OPN populations were not spatially discrete in the PCX. Despite that intermingling, individual cells were rarely double-labeled. The data suggest strongly that the PCX neurons that receive nontopographically defined and overlapping afferent inputs from the olfactory bulb segregate into a minimum of two parallel output circuits that independently provided olfactory input to subdivisions of the OFC.

Table 1. Distribution of LO-OPN in the PCX

	Rostral aPCX				Middle/caudal aPCX		pPCX	
Animal	Region 1	Region 2	Region 3	Region 4	Region 1	Region 2	Region 1	Region 2
020713	397 (62%)	43 (7%)	26 (4%)	171 (27%)	154 (73%)	56 (27%)	15 (58%)	11 (42%)
021213	163 (51%)	27 (8%)	5 (2%)	123 (39%)	336 (72%)	131 (28%)	26 (59%)	18 (41%)
050713	102 (54%)	21 (11%)	4 (2%)	62 (33%)	125 (73%)	47 (27%)	1 (100%)	0 (0%)
052113	226 (70%)	17 (5%)	22 (7%)	57 (18%)	202 (82%)	43 (18%)	0 (0%)	0 (0%)
053113	229 (73%)	22 (7%)	5 (2%)	56 (18%)	129 (88%)	18 (12%)	1 (100%)	0 (0%)

Discussion

A major aim of research in central odor processing is to understand the principles regarding odor coding in PCX, a region lacking an apparent afferent spatial topography, as is found in other primary sensory cortices (36, 37). Although there is precise laminar organization (38), a topographical organization in both afferent and association fiber targeting within the PCX has never been established (12, 20–22). Odor stimuli are represented in the PCX by sparse, spatially overlapping, and distributed activity patterns (13–15). However, the results presented here demonstrate that although the afferent input is nontopographically organized, a spatial organization emerges from examination of the efferent circuits of the PCX. The pyramidal cells projecting to a specific cortical target are not evenly distributed, but rather are compartmentally distributed in the dorsal–ventral region of the PCX (Fig. 2). The neurons projecting to the LO are strongly localized to the most rostral subdivision of the PCX, whereas the neurons projecting to the neighboring AI are more broadly distributed throughout the anterior–posterior region of the PCX (Fig. 3 *A*–*C*). The evidence that double-labeling from the LO and the AI injections was sparse suggests that the target-dependent output circuits are target-specific as well (Fig. 3 *D* and *E*).

Data regarding efferent topography of the PCX has been shown in rats (30, 31). Although not highly specified, the patterns of the retrogradely labeled cells presented in the PCX showed both a bimodal distribution (regions 1 and 4 preference of the rostral aPCX) and a ventral domination (region 1 preference of the remaining PCX) (Fig. 2 *D* and *H*) following wheat germ agglutinin–horseradish peroxidase injections into the OFC subdivisions (30). A specific subdivision in the ventral aPCX (comparable to region 1 of the present study) has also been identified by Ekstrand et al. for its strong neuronal projection to the OFC (31). These studies together suggest a location-based efferent system in the PCX. Our data confirm and extend these previous findings. Furthermore, the evidence that a large portion of LO- and AI-OPNs intermingled within the same cortical domains provides an unexpected insight into this location-based efferent system: Spatial segregation between OPN populations is not required.

The disparity in anterior–posterior distributions of LO- and AI-OPNs suggests that the PCX output to each of its targeting areas may be unique and target-specific. Given the distributed divergent and convergent afferent projections onto individual PCX neurons, two output circuits containing random OPN collections are likely representing similar odor stimuli and generating similar olfactory output. However, data from recent studies indicated that odors are differentially encoded within the two PCX subdivisions (39–42), with neurons of aPCX encoding more analytical odor features such as structure-based odor identity and pPCX neurons encoding more associational information such as odor similarity and categories. Therefore, neuronal populations with different aPCX/pPCX ratios could potentially generate outputs with unique qualities. In the present study, for example, output from LO-OPNs may contain preferentially odor identity information, whereas the olfactory percept generated by AI-OPNs may be more "balanced." With this hypothesis in mind, it is possible that the differential olfactory outputs may reflect the roles of the LO and the AI in odor-guided behaviors and olfactory associative learning. More data from neural track tracing, functional imaging, and animal behavioral studies will be needed to test these hypotheses.

The efferent PCX topography matches strikingly well with patterns of OFC-to-PCX (top–down) projection. aPCX receives projections from cells of both LO and AI, whereas pPCX receives projections largely from AI (43, 44). In addition, labeled axons from subdivisions of OFC show similar bimodal distribution and ventral domination within the aPCX (44). Therefore, the reciprocal connections between subdivisions of PCX and OFC appear to be precise and specific.

The extreme organization of the peripheral olfactory system, in which particular odorant receptors appear to direct the formation of a segregated map of function in the glomeruli on the surface of the olfactory bulb, has given rise to numerous models of topographical odor representations. Piriform cortex would seem to be the natural location for the processing of this topographical olfactory map to form odor objects, except that anatomical and physiological features of both afferent and associational fiber systems indicate a highly distributed organization (15, 20–22, 25, 26). The results presented here suggest that PCX does have a topographic organization but that it is more clearly understood through output rather than input. That is, populations of PCX neurons are segregated depending on where their axons are projecting and not on the input they are receiving.

Indeed it would appear that most pyramidal and semilunar cells, the OPNs of the PCX, may get very similar input from the periphery and that a relatively small number of them sampling this input is sufficient to produce a coherent projection to higher centers for further processing. As few as 500 PCX neurons are sufficient to encode odor identity (45), yet a given odor may

Table 2. Distribution of AI-OPN in the PCX

	Rostral aPCX				Middle/caudal aPCX		pPCX	
Animal	Region 1	Region 2	Region 3	Region 4	Region 1	Region 2	Region 1	Region 2
020713	62 (33%)	21 (11%)	9 (5%)	95 (51%)	360 (72%)	141 (28%)	327 (77%)	96 (23%)
021213	86 (36%)	32 (13%)	7 (3%)	113 (47%)	427 (67%)	208 (33%)	179 (78%)	50 (22%)
050713	44 (33%)	24 (18%)	8 (6%)	56 (42%)	193 (65%)	104 (35%)	23 (92%)	2 (8%)
053113	135 (52%)	33 (13%)	5 (2%)	87 (33%)	321 (72%)	125 (28%)	143 (79%)	37 (21%)

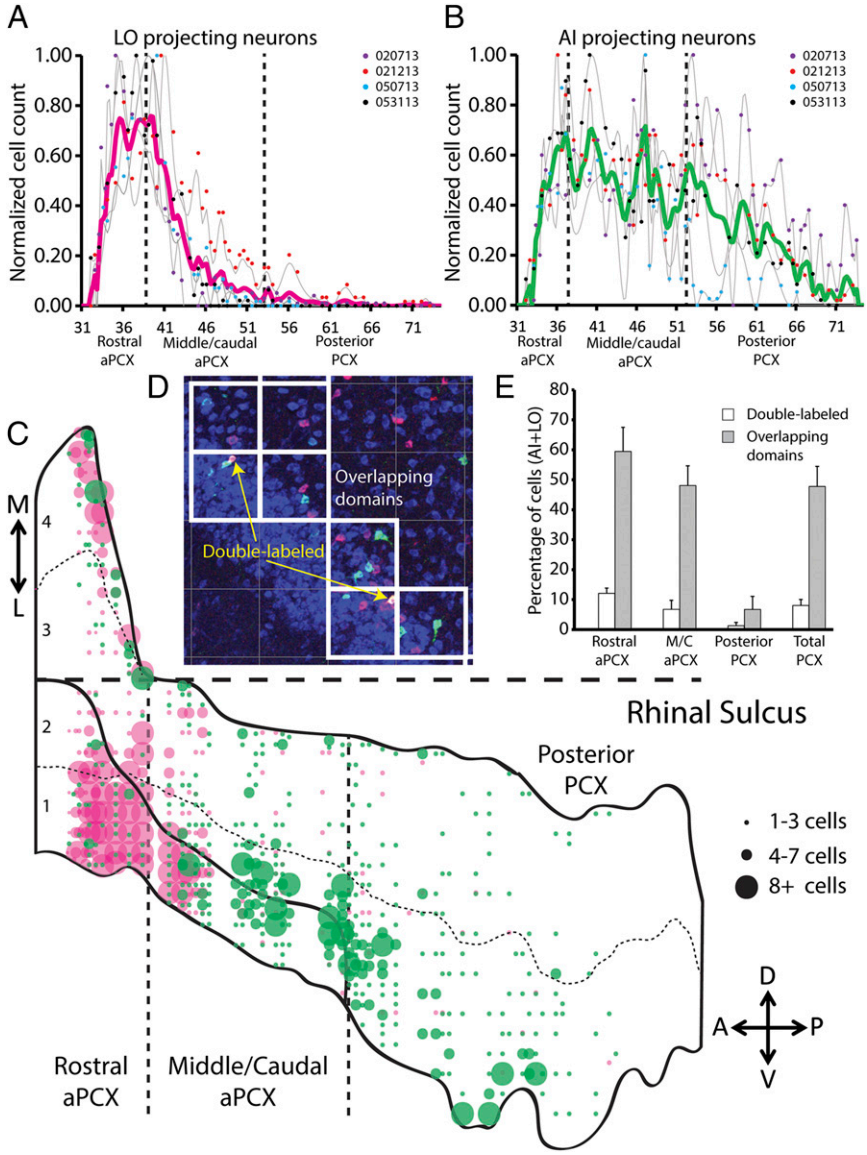

Fig. 3. The OPN distributions on the anterior–posterior axis of the PCX. (*A* and *B*) Cell-count data of the coronal sections were normalized and plotted for each animal and presented by dots of different colors. The smoothed distribution patterns (gray lines) of each animal were also normalized (*Materials and Methods*). The thick pink and green lines represent the average LO-OPN and AI-OPN distributions on the anterior–posterior axis. The dashed lines separate subdivisions of the PCX. (*C*) Distribution patterns of the LO-OPNs (pink) and the AI-OPNs (green) from mouse 020713, presented by three dot sizes. The dashed vertical lines mark the boundaries between the rostral aPCX, the middle/caudal aPCX, and the pPCX. Regions 1–4 are separated by thin dashed lines. (*D*) An example of the AI (green, CTB-555) and LO (pink, CTB-647) projecting neurons that are within overlapping domains (white boxes) of the PCX. Neurons projecting to both OFC areas are labeled by both CTB-555 and CTB-647 (marked by the yellow arrows). (*E*) Average percentages of the OPNs that are double-labeled (white bars) and within overlapping domains (gray bars) in the three PCX subdivisions. Error bars, standard error.

activate thousands of PCX neurons (13, 15). It may be that specific features of the odor input are extracted by these different populations such that higher cortices receive slightly different versions of the odor input and that an integration stage, where the final percept is delivered to consciousness, must be imagined beyond the PCX. Whatever or wherever that mechanism may turn out to be, it now seems clear that the odor "map" suggested for the olfactory bulb is not required or used for perception. The transformation of a chemical or set of chemicals into an odor percept may be widely distributed in multiple brain areas.

Materials and Methods

CTB Injection. We used adult C57BL/6J male mice (4–10 wk old) bred in the animal facility of Columbia University and housed on a 12-h light/dark cycle, with food and water available ad libitum. Animal care protocols and all experiments were approved by the Columbia University Institutional Animal Care and Use Committee and were in accordance with National Institutes of Health guidelines.

The animal was anesthetized by injecting ketamine/xylazine (initial dose, 90 mg/10 mg/kg) intraperitoneally. A deeply anesthetized animal was placed into the stereotaxic device with a heating unit underneath its abdomen. One burr hole (~3 mm × 2 mm) on the dorsal surface of the skull was created by a craniotomy. Dura mater was carefully removed using a new 19 G needle. The ketamine/xylazine boosters (20% initial dose) were provided to the animal during the surgery as needed.

For the retrograde tracing, two CTB fluorescent conjugates, Alexa Fluor 555 and 647 (Life Technologies), were dissolved with phosphate buffer saline (pH 7.4) to make 0.5% solutions. The injection micropipettes were pulled from borosilicate glasses (OD, 1.2 mm; ID, 0.6 mm), and their tips were broken to generate an opening ~20 μm in diameter. The CTB loaded micropipette was positioned to either coordinates (for the AI, 2.46 mm anterior and 2.10

mm lateral to the bregma; for the LO, 2.46 mm anterior and 1.50 mm lateral to the bregma) and lowered 2.00 mm (LO) or 2.15 mm (AI) from the surface. The CTB conjugates were injected by iontophoresis (33) by pulses (+4 μA) with a 7 s on/off cycle for 30–45 min to create an injection site <200 μm in diameter (Fig. 1*A*). After injection, the micropipette stayed in the same position for 1 min. During micropipette extraction, a constant negative current (–0.5 μA) was provided to minimize tracer leakage in the track. We used bone wax (World Precision Instruments) to seal the burr hole and Vetbond (3M) to close the wound.

A total of 18 male mice were used in this study, and five of them were selected for further examination based on location and precision of label injections. Three mice (020713, 021213, and 053113) had CTB-555 in the AI and CTB-647 in the LO. To ensure each dye does not preferentially label one population of OPNs, one mouse (050713) had CTB-555 in the LO and CTB-647 in the AI. One mouse (052113) had CTB-555 in the LO and no tracer in the AI. To test the efficacy of colabeling, one mouse was simultaneously injected with a mixture of both tracers in equal amounts.

Data Acquisition and Analysis. The mice were perfused intracardially with 4% (wt/vol) paraformaldehyde 7 d after tracer injections. Coronal brain cryosections (25 μm thick) were mounted on the gelatin-coated slides into three series and stained with NeuroTrace 435/455 Blue fluorescent Nissil stain (1:150 dilution) (Life Technologies). For each animal, only one series of the brain sections was imaged with a Zeiss LSM 700 confocal microscope. All images were acquired using Zen 2010 (Carl Zeiss Inc.), which combined multiple scanned images (319.8 μm × 319.8 μm each) with 3~4 focal planes and superimposed them into one composite image. The PCX images were first registered on an anterior–posterior axis using the Allen mouse brain atlas (46). The PCX was divided into three subdivisions: the rostral aPCX (position 31–39), the middle/caudal aPCX (position 40–54), and the pPCX (position 55–74). A CTB-positive cell was confirmed by seeing the colabeling of the CTB and NeuroTrace Blue that labeled Nissl bodies in the cytoplasm of a cell. Using this method, we manually counted the CTB-positive cells in layers II/III of the PCX. The cells in the endopiriform nucleus were not included in the analysis.

To generate an anterior–posterior distribution pattern of the OPNs in each animal, the cell-count number of each coronal section was first registered on the anterior–posterior axis. A smoothed line that connects each data point was generated using spline algorism in Matlab (MathWorks). Because each animal had a unique retrograde tracing condition, to compare the patterns of individual animals, both the data points and the smoothed lines were normalized by dividing each data point/lines with the biggest value of the datasets.

ACKNOWLEDGMENTS. The authors would like to thank Natasha Kharas for help on image acquisition and immunochemistry and Elizabeth H. Krusch and Nina Deoras for preparing the data.

1. Wilson DA, Sullivan RM (2011) Cortical processing of odor objects. *Neuron* 72(4): 506–519.
2. Gottfried JA (2010) Central mechanisms of odour object perception. *Nat Rev Neurosci* 11(9):628–641.
3. Neville KR, Haberly L (2004) Olfactory cortex. *The Synaptic Organization of the Brain*, ed Shepherd GM (Oxford Univ Press, New York), 5th Ed, pp 415–454.
4. Buck L, Axel R (1991) A novel multigene family may encode odorant receptors: A molecular basis for odor recognition. *Cell* 65(1):175–187.
5. Zhang X, Zhang X, Firestein S (2007) Comparative genomics of odorant and pheromone receptor genes in rodents. *Genomics* 89(4):441–450.
6. Mombaerts P, et al. (1996) Visualizing an olfactory sensory map. *Cell* 87(4): 675–686.
7. Ressler KJ, Sullivan SL, Buck LB (1994) Information coding in the olfactory system: Evidence for a stereotyped and highly organized epitope map in the olfactory bulb. *Cell* 79(7):1245–1255.
8. Vassar R, et al. (1994) Topographic organization of sensory projections to the olfactory bulb. *Cell* 79(6):981–991.
9. Fried HU, Fuss SH, Korsching SI (2002) Selective imaging of presynaptic activity in the mouse olfactory bulb shows concentration and structure dependence of odor responses in identified glomeruli. *Proc Natl Acad Sci USA* 99(5):3222–3227.
10. Xu F, et al. (2003) Odor maps of aldehydes and esters revealed by functional MRI in the glomerular layer of the mouse olfactory bulb. *Proc Natl Acad Sci USA* 100(19): 11029–11034.
11. Soucy ER, Albeanu DF, Fantana AL, Murthy VN, Meister M (2009) Precision and diversity in an odor map on the olfactory bulb. *Nat Neurosci* 12(2):210–220.
12. Price JL (1973) An autoradiographic study of complementary laminar patterns of termination of afferent fibers to the olfactory cortex. *J Comp Neurol* 150(1):87–108.
13. Illig KR, Haberly LB (2003) Odor-evoked activity is spatially distributed in piriform cortex. *J Comp Neurol* 457(4):361–373.
14. Rennaker RL, Chen CF, Ruyle AM, Sloan AM, Wilson DA (2007) Spatial and temporal distribution of odorant-evoked activity in the piriform cortex. *J Neurosci* 27(7): 1534–1542.
15. Stettler DD, Axel R (2009) Representations of odor in the piriform cortex. *Neuron* 63(6):854–864.
16. Lei H, Mooney R, Katz LC (2006) Synaptic integration of olfactory information in mouse anterior olfactory nucleus. *J Neurosci* 26(46):12023–12032.
17. Kay RB, Meyer EA, Illig KR, Brunjes PC (2011) Spatial distribution of neural activity in the anterior olfactory nucleus evoked by odor and electrical stimulation. *J Comp Neurol* 519(2):277–289.
18. Poo C, Isaacson JS (2009) Odor representations in olfactory cortex: "Sparse" coding, global inhibition, and oscillations. *Neuron* 62(6):850–861.
19. Carmichael ST, Clugnet MC, Price JL (1994) Central olfactory connections in the macaque monkey. *J Comp Neurol* 346(3):403–434.
20. Sosulski DL, Bloom ML, Cutforth T, Axel R, Datta SR (2011) Distinct representations of olfactory information in different cortical centres. *Nature* 472(7342):213–216.
21. Ghosh S, et al. (2011) Sensory maps in the olfactory cortex defined by long-range viral tracing of single neurons. *Nature* 472(7342):217–220.
22. Johnson DM, Illig KR, Behan M, Haberly LB (2000) New features of connectivity in piriform cortex visualized by intracellular injection of pyramidal cells suggest that "primary" olfactory cortex functions like "association" cortex in other sensory systems. *J Neurosci* 20(18):6974–6982.
23. Haberly LB, Price JL (1978) Association and commissural fiber systems of the olfactory cortex of the rat. *J Comp Neurol* 178(4):711–740.
24. Poo C, Isaacson JS (2011) A major role for intracortical circuits in the strength and tuning of odor-evoked excitation in olfactory cortex. *Neuron* 72(1):41–48.
25. Franks KM, et al. (2011) Recurrent circuitry dynamically shapes the activation of piriform cortex. *Neuron* 72(1):49–56.
26. Miyamichi K, et al. (2011) Cortical representations of olfactory input by trans-synaptic tracing. *Nature* 472(7342):191–196.
27. Davison IG, Ehlers MD (2011) Neural circuit mechanisms for pattern detection and feature combination in olfactory cortex. *Neuron* 70(1):82–94.
28. Price JL (1985) Beyond the primary olfactory cortex—Olfactory-related areas in the neocortex, thalamus and hypothalamus. *Chem Senses* 10(2):239–258.
29. Price JL, Slotnick BM, Revial MF (1991) Olfactory projections to the hypothalamus. *J Comp Neurol* 306(3):447–461.
30. Price JL, et al. (1991) Olfactory input to the prefrontal cortex. *Olfaction: A Model System for Computational Neuroscience*, eds Davis JL, Eichenbaum H (The MIT Press, Cambridge, MA), pp 101–120.
31. Ekstrand JJ, et al. (2001) A new subdivision of anterior piriform cortex and associated deep nucleus with novel features of interest for olfaction and epilepsy. *J Comp Neurol* 434(3):289–307.
32. Schoenbaum G, Setlow B, Nugent SL, Saddoris MP, Gallagher M (2003) Lesions of orbitofrontal cortex and basolateral amygdala complex disrupt acquisition of odor-guided discriminations and reversals. *Learn Mem* 10(2):129–140.
33. Conte WL, Kamishina H, Reep RL (2009) Multiple neuroanatomical tract-tracing using fluorescent Alexa Fluor conjugates of cholera toxin subunit B in rats. *Nat Protoc* 4(8): 1157–1166.
34. Ray JP, Price JL (1992) The organization of the thalamocortical connections of the mediodorsal thalamic nucleus in the rat, related to the ventral forebrain-prefrontal cortex topography. *J Comp Neurol* 323(2):167–197.
35. Krettek JE, Price JL (1977) Projections from the amygdaloid complex to the cerebral cortex and thalamus in the rat and cat. *J Comp Neurol* 172(4):687–722.
36. Formisano E, et al. (2003) Mirror-symmetric tonotopic maps in human primary auditory cortex. *Neuron* 40(4):859–869.
37. Casagrande V, Kaas J (1994) The afferent, intrinsic, and efferent connections of primary visual cortex in primates. *Primary Visual Cortex in Primates, Cerebral Cortex*, eds Peters A, Rockland K (Springer, New York), Vol 10, pp 201–259.
38. Luskin MB, Price JL (1983) The laminar distribution of intracortical fibers originating in the olfactory cortex of the rat. *J Comp Neurol* 216(3):292–302.
39. Gottfried JA, Winston JS, Dolan RJ (2006) Dissociable codes of odor quality and odorant structure in human piriform cortex. *Neuron* 49(3):467–479.
40. Kadohisa M, Wilson DA (2006) Separate encoding of identity and similarity of complex familiar odors in piriform cortex. *Proc Natl Acad Sci USA* 103(41):15206–15211.
41. Roesch MR, Stalnaker TA, Schoenbaum G (2007) Associative encoding in anterior piriform cortex versus orbitofrontal cortex during odor discrimination and reversal learning. *Cereb Cortex* 17(3):643–652.
42. Calu DJ, Roesch MR, Stalnaker TA, Schoenbaum G (2007) Associative encoding in posterior piriform cortex during odor discrimination and reversal learning. *Cereb Cortex* 17(6):1342–1349.
43. Datiche F, Cattarelli M (1996) Reciprocal and topographic connections between the piriform and prefrontal cortices in the rat: A tracing study using the B subunit of the cholera toxin. *Brain Res Bull* 41(6):391–398.
44. Illig KR (2005) Projections from orbitofrontal cortex to anterior piriform cortex in the rat suggest a role in olfactory information processing. *J Comp Neurol* 488(2):224–231.
45. Choi GB, et al. (2011) Driving opposing behaviors with ensembles of piriform neurons. *Cell* 146(6):1004–1015.
46. Lein ES, et al. (2007) Genome-wide atlas of gene expression in the adult mouse brain. *Nature* 445(7124):168–176.